J Polym Res (2015) 22: 82
DOI 10.1007/s10965-015-0730-6

ORIGINAL PAPER

Variation of core-shell structural particles and their toughening behavior in poly (vinyl chloride) (PVC) matrix

Shuting Wu [1,2] · Ming Chen [1,2] · Guangfeng Wu [1,2] · Chao Zhou [1,2]

Received: 3 August 2014 / Accepted: 8 April 2015 / Published online: 17 April 2015

Abstract Three methyl methacrylate-butadiene-styrene (MBS) core-shell particles with different structures, namely, "salami," "core-shell," and "multi-layer," were synthesized in this work. All the MBS particles were designed with the same defined chemical composition, which is a prerequisite for producing transparent blends with poly (vinyl chloride) (PVC). This work focused on the influence of the internal structure of core-shell particles on the properties of the PVC/MBS blends. Results of the dynamic mechanical analysis illustrated that the different internal structures greatly affected the glass transition temperature (T_g) of the rubbery phase and the storage modulus of the core-shell particles. The test results on the mechanical properties showed that the PVC/MBS blend with the "multi-layer" modifier had the highest tensile stress and fracture strain values, the lowest brittle-ductile transition (BDT) temperature, and the highest impact strength at a higher temperature. With the different structure, both cavitation and debonding from the matrix were observed, which relieve the triaxial tension and promote the shear yielding of the PVC matrix. The optical property showed that the PVC/MBS blend with the "core-shell" modifier had a higher transparency than the other blends.

Keywords MBS · Internal structure · Core-shell · Brittle-ductile transition temperature · Toughening

✉ Chao Zhou
zhouc@mail.ccut.edu.cn

[1] Engineering Research Center of Synthetic Resin and Special Fiber, Ministry of Education, Changchun University of Technology, Changchun 130012, China

[2] Research Institute of Jilin Petrochemical Company, Petro China, Jilin, China

Introduction

It is important to increase the toughness of polymers for many practical applications. The addition of rubbery phase into a polymeric material is commonly employed to increase the toughness of polymeric materials [1]. Rubber toughened plastics were first manufactured in the late 1940s and have since been studied very extensively. It is often assumed that rubber toughening is synonymous with addition of rubber particles [2]. Nowadays, many other techniques contribute to knowledge of rubber toughening, so that the ways in which rubber content, rubber particle morphology, shape and size, rubber particle cavitation, and strain rate and temperature affect fracture behavior can be studied [1–7]. Despite the frequent use, the toughening mechanisms of this are in debate. The main energy dissipative processes in rubber toughened thermoplastics are massive matrix crazing, cavitation, and multiple localized shear bands initiated by the particles [3]. The morphology of the toughening particles also has a large influence on the physical and mechanical behavior of the resulting toughened matrix [8]. To improve compatibility between the rubber particles and the plastics matrix, so called core-shell impact modifiers have been developed [9–13]. Riess and Echte [14, 15] used electron microscopy shown that the novel materials differ in several ways from the more tradition HIPS grades. The two most obvious differences are similar particle size and a distinctive morphology with in the rubber particles. Whereas the rubber particles in established HIPS have a "salami" structure, with numerous polystyrene sub-inclusions embedded in a continuous rubbery phase, the newer type of rubber particles formed from block copolymers have a "core-shell" structure, a thin spherical shell of rubber encloses a single polystyrene inclusion.

Core-shell structured particles, which comprise rubbery and glassy layers, have the distinct advantage of allowing

independent control of the composition, morphology, size and properties [16, 17]. Variation of the core-shell internal structural particles may affect the properties of the host matrix. Gao et al.[18] studied the rubber particles of PS/PB-g-PS (AIBN) included a large scale of PS sub-inclusion, which was able to promote the toughness of modified PS more effective than the rubber particles of PS/PB-g-PS (redox) which included some microphase PS zones. Dong et al.[19] reported that the high-performance bio-sourced PLLA/PA11 blends have been fabricated with the incorporation of reactive EGMA-g-AS rubber. A fine salami structure with the EGMA-g-AS exclusively dispersed in the PLLA domains endowed blends with the highest ductility. Depending on the polymerization parameters and conditions [16, 20, 21], the core-shell particles may contain several alternate layers of rubbery and glassy polymer and the properties of the rubber itself can be altered. Lovell et al.[22] prepared multiple-layer particles as impact modifiers for PMMA. Nelliappan et al.[23] prepared multilayered particles by emulsion polymerization and the three-layer particles were more effective in toughening poly (methyl methacrylate) (PMMA) than two-layer particles. Schneider et al.[24, 25] studied that the performance of NR based core-shell particles in PS blends could be considerably increased when rigid PS sub-inclusions were introduced into the soft rubbery core.

Our previous work [26–28] focused on the effects of the monomer addition method, initiators, and the arrangement of styrene on the internal structure of MBS core-shell particles, hard/soft/hard three-layer MBS particles, and the properties of PVC/MBS blends.

This work studied the relationship between the internal structure of the impact modifiers and the mechanical and optical properties of the PVC/MBS blends.

Experiment

Materials

Styrene (St) and methyl-methacrylate (MMA) (supplied by the Jilin Chemical Company, Jilin City, China) were used as monomers. Poly-butadiene (PB), styrene-butadiene rubber (SBR), and poly-styrene-butadiene (PSB) were supplied by the Jilin Chemical Company and were used as seed latex. Cumene hydro peroxide ferrous salt (CHP-Fe^{2+}) was employed as the initiator in this work. Distilled deionized water was used in all polymerizations. PVC resin was supplied by the Jilin Chemical Company, China. The M_w and M_n of the PVC resin were 72,000 and 40,000 g/mol, respectively.

Synthesis of MBS core-shell particles

The MBS copolymers were obtained using the emulsion polymerization method. The process consisted of two basic stages: the synthesis of the seed latex and the grafting of the monomers on the core by continuous feeding. All the MBS samples in this study were designed with the same chemical composition (M/B/S=30/49/21). MBS-1 had a PB core, first the St and then the MMA were grafted on the core as shell. MBS-2 had an SBR core and a grafted shell of MMA monomer. MBS-3 had a hard poly-styrene (PS) inner core, an interim soft PB layer, and a grafted hard external MMA layer. The recipe for the synthesis of the MBS core-shell particles is listed in Table 1. In the preparation process, sodium pyrophosphate (SPP), dextrose (DX), and iron (II) sulfate ($FeSO_4$) were used without further purification. An oil-soluble initiator, cumene hydro peroxide (CHP), was used in combination with a redox system. The emulsion polymerization was performed in a 1 L three-neck glass reactor with a reflux, inlet nitrogen at 70 °C under alkaline conditions of pH 10. First, the distilled deionized water, seed latex, initiator, and KOH were added into the glass reactor and stirred for 5 min under nitrogen. Second, the monomers mixed with the initiator were added in two stages. In the grafting process, the monomers were added separately: first the St and then the MMA for MBS-1. The reaction was conducted for 4 h. MMA was grafted on MBS-2 and MBS-3, so that the reactions were conducted for 2 h. After adding 10 g of antioxidant solution, the reactor temperature was decreased to 60 °C, and the reaction was completed. A magnesium sulfate ($MgSO_4$) solution was added to facilitate the coagulation of the latex obtained from the emulsion polymerization and to yield a loose aggregation of the particles. The polymers were then dried in a vacuum oven at 60 °C for 24 h before use.

Characterizations

The particle size and particle size distribution of the core and MBS in the emulsion latex were characterized by dynamic light scattering using an American Brookhaven 90 Plus particle size analyzer. The dynamic storage modulus and tanδ of MBS were measured using a dynamic mechanical analyzer (DMA242, Germany) at a frequency of 10 Hz. The specimen bar had the size of $30\times10\times1$ mm^3 and a heating rate of 3 °C/min at a temperature ranging from −100 to 150 °C. Blends of 100 phr PVC, 10 phr MBS, and 2 phr heat stabilizers (Octyltin Mercaptide) were compounded by roll-milling

Table 1 Recipe for synthesis of MBS core-shell particles

Particle	M/B/S	Core			Shell	
		PB(g)	SBR(g)	PSB(g)	St(g)	MMA(g)
MBS-1	30/49/21	49	-	-	21	30
MBS-2	30/49/21	-	70	-	-	30
MBS-3	30/49/21	-	-	70	-	30

at 165 °C for 5 min. The films obtained were pressed into sheets by compression molding at 185 °C for 5 min. The thickness was set at 1 mm for the tensile and transparency tests and 5 mm for the Izod impact tests. The notched Izod impact strength of the PVC/MBS blends was determined according to ASTM D256 on a XJU-22 apparatus. The specimens ($63.5\times12.7\times5$ mm^3) were cut from the compression-molded sheet, and the impact tests were conducted at different temperatures ranging from −10 to 25 °C to show the brittle-ductile transition (BDT) of the blends. In this study, the Izod impact strength was an average of five measurements per sample at each temperature. All the tensile specimens were molded into a dumb-bell type whose dimensions in the parallel part were 30 mm in length. The tensile tests were conducted on an Instron 3365 electrical testing machine at a constant crosshead speed of 50 mm/min at 23 °C. The TEM samples were microtomed from the undeformed zone of the PVC/MBS blends to examine the dispersed morphology of MBS in the matrix and the stress-whitening zone immediately beneath the impact fracture surface to examine the deformation behavior. The samples were then cut into ultrathin sections with a thickness of 60 nm using a microtome at −100 °C and were stained with osmium tetroxide (OsO_4) vapor to enhance the contrast among their components before characterization. A JEM-1011 transmission electron microscope was operated at 100 kV. The transmittances of the blends were measured using a photometer (WGW-1) at room temperature. The specimens had plane-parallel surfaces free of dust and internal voids. The specimens with a thickness of 1 mm were cut from the compression-molded sheet, and the size of each test specimen was sufficiently large to cover the entrance port of the sphere.

Results and discussion

Characteristics of MBS

To investigate the influence of the internal structure of MBS on the properties of the blends, three MBS samples were designed with the same chemical compositions in this study. Table 2 gives the characteristics of the core-shell MBS particles.

Emulsion polymerization is a well-known technique for preparing latex polymers with defined structures [29–31]. The structural schemes of three core-shell particles in our study were list in Fig. 1.

TEM is a necessary measure used in studying the dispersion state of MBS particles in a PVC matrix and the internal structure of the MBS particles. Stained rubber particles can be dispersed well in the matrix because the grafted MMA is miscible with the PVC matrix. Therefore, in the TEM, the external shell cannot be distinguished from the matrix. For MBS-1, the St was fed in a semi-continuous feeding process, while parts of the St monomer was swollen into the PB rubbery phase for the formation of many small sub-inclusions in it, called the "salami" structure. In the MBS-2, the entire St monomer was copolymerized with butadiene (Bd), and the core of MBS was the copolymer of SBR. Thus, no obvious sub-inclusions formed in it. MBS-3 was the hard/soft/hard three-layer particles. Given that OsO_4 was used to stain the double bonds of Bd, the internal PS glassy core was relatively light gray, and the middle soft PB layer was dark. Figure 2 shows the dispersed state of MBS in the PVC matrix and the internal structure of the MBS particles.

The DMA curve of MBS gives two tan δ peaks: one, in the low temperature region, belongs to the rubbery phase, and the other, in the higher temperature region, belongs to the glass shell and copolymer phases. In the following, only the glass transition of the rubbery phase is discussed. As Fig. 3 shows, the MBS-3 with a larger "sub-inclusion" had a lower T_g than MBS-1 and MBS-2. In the low temperature region, the value of the maximum tan δ increases with the rubber volume fraction [14, 32, 33]. The increase in the maximum tanδ of the three MBS samples can be explained by the increase in the effective volume fraction of the rubber particles. The three MBS samples have a similar particle size. In the MBS-2, the entire St is copolymerized with Bd, and the shell contains only MMA, as shown in Fig. 1 (b), thereby leading to the maximum rubber volume fraction. This may be the main reason for the increase in the value of the maximum tan δ. The temperature dependence of the dynamic storage modulus recorded for MBS is presented in Fig. 4.

Mechanical properties of PVC/MBS blends

Impact strength testing is one of the most widely used methods for investigating polymer toughness. As Fig. 5 shows, the Izod impact strength is plotted as a function of temperature for the three different PVC/MBS blends with

Table 2 Characteristics of the MBS particles employed in this study

Particle	M/B/S	Structure of MBS	St/Bd in the inner core	Particle size of core latex (nm)	Particle size of MBS latex (nm)
MBS-1	30/49/21	salami	0/100	256.5	271.5
MBS-2	30/49/21	core-shell	30/70	236.2	251.6
MBS-3	30/49/21	multi-layer	100/0	222.5	262.4

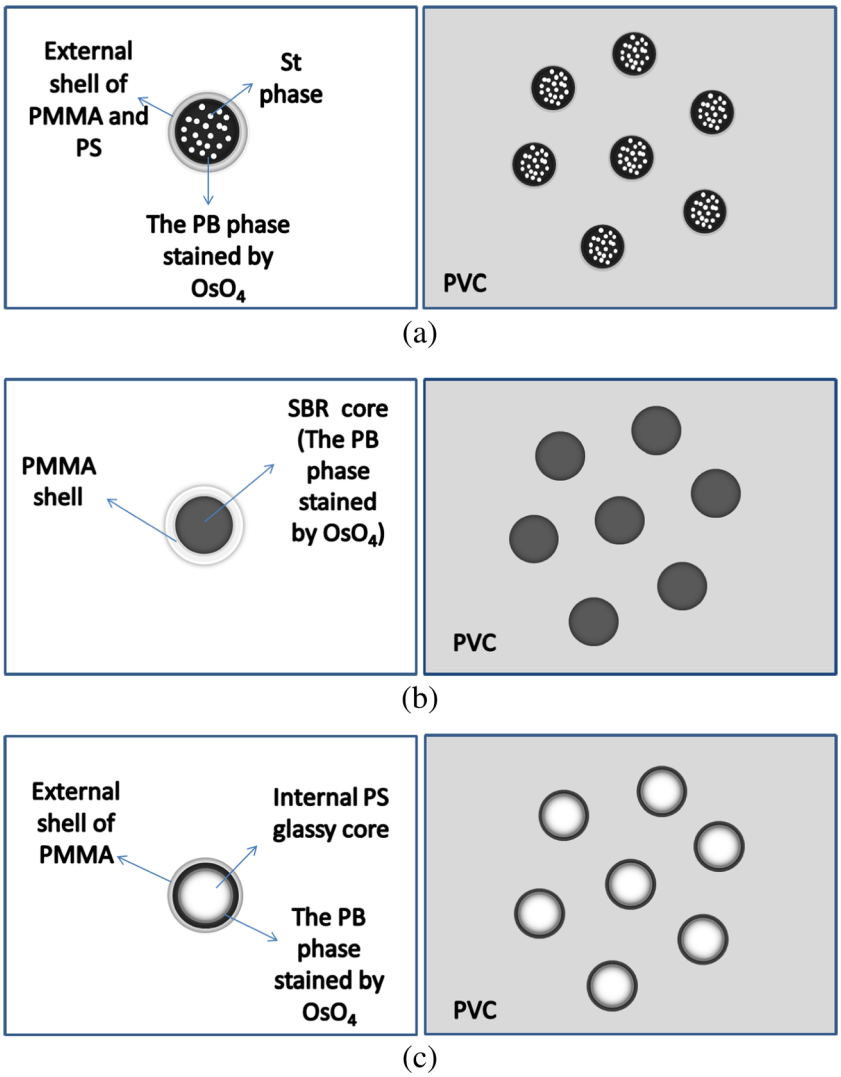

Fig. 1 The scheme of Core-shell particles and their blends with PVC: **a** salami (MBS-1), PVC/MBS-1; **b** core-shell (MBS-2), PVC/MBS-2; **c** multi-layer (MBS-3), PVC/MBS-3

the same rubber content (10 phr MBS). They are S-shaped. At a low temperature, all the blends had notched impact strengths of 100–350 J/m, independent of the type of MBS modifier used. The fracture samples only showed slight intensive stress whitening in a small volume of the material near the notch tip. At a higher temperature, all the blends had notched impact

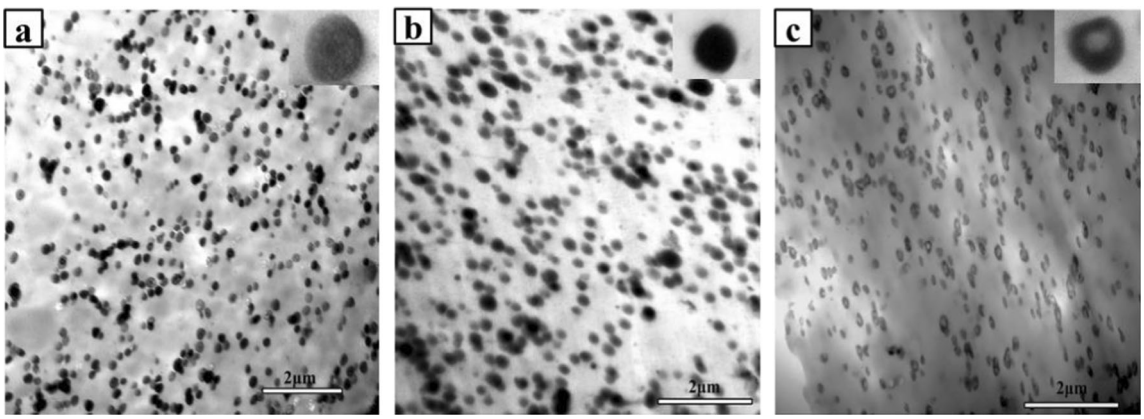

Fig. 2 TEM micrograph of the dispersion of the PVC/MBS blends and internal structure of the MBS: **a** PVC/MBS-1; **b** PVC/MBS-2; **c** PVC/MBS-3

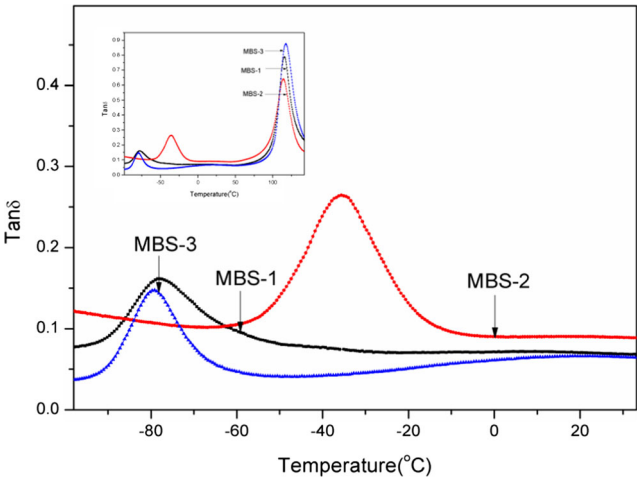

Fig. 3 tanδ as a function of temperature for different structure of MBS

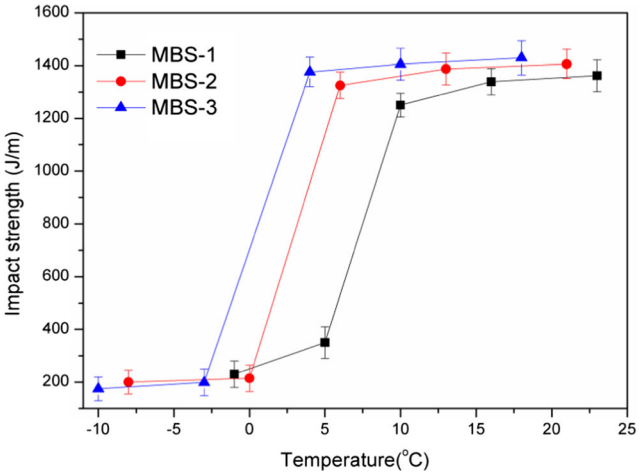

Fig. 5 Izod impact strength as a function of temperature for three different PVC/MBS blends with nearly the same particle size

strength between 1200 and 1400 J/m. The fracture samples showed intensive stress whitening in a large volume of the test sample. The influence of the variety of the internal structure of the MBS particles on the impact behavior of the blends can be related to the effective rubber volume fraction and dynamic storage of MBS. As Figs. 3 and 4 show, MBS-3 had the highest value of dynamic storage modulus; it also had a higher impact strength at a high temperature; and its brittle ductile transition (BDT) temperature shifted to a lower temperature.

Many studies have shown that the addition of rubber can lead to a significant enhancement in toughness but sacrifice of stiffness and strength [34, 35]. The stress–strain curves of PVC/MBS blends were given in Fig. 6. The blends with "multi-layer" particles MBS-3, have a yield stress value about 52 MPa, which is rather higher than the others. The higher value of the tensile stress is directly related to multi-layer structure and the presence of hard PS glassy domains in the core, which acted as stiffening agents.

Deformation mechanism of the PVC/MBS blends

Sufficient evidence of rubber particle cavitation and matrix shear yielding was obtained with both optical and electron microscopes by Person and Yee [36–38]. As they proposed, shear deformation can be initiated by the stress concentrations associated with rubber particles, but hydrostatic tensile stresses due to notch and crack tip constraints mean that this occurs on a very limited scale. Cavitation of the rubber particles releases these hydrostatic tensile stresses and encourages the shear yielding to proceed. Lazzeri and Bucknall [39] studied the model based on a critical stored energy criterion as following:

$$U_r(r) = \frac{2}{3}\pi R^3 k_r \left(\Delta V_R - \frac{r^3}{R^3}\right)^2 + 4\pi r^2 \Gamma + 2\pi r^3 G_r F(\lambda_f)$$

Where G_r and K_r are the shear modulus and bulk modulus of the rubber, ΔV is the volume strain in the rubber

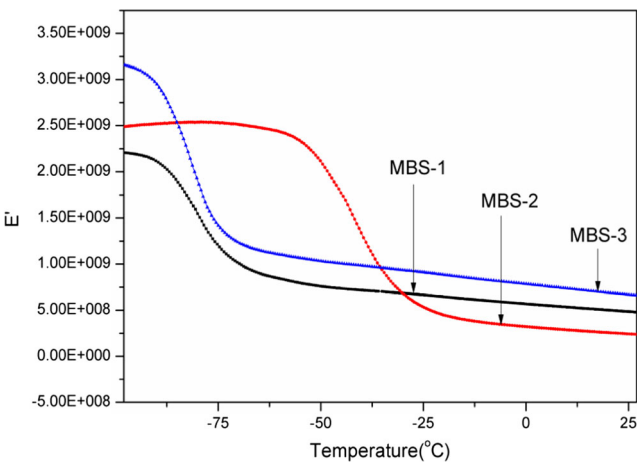

Fig. 4 E' as a function of temperature for MBS

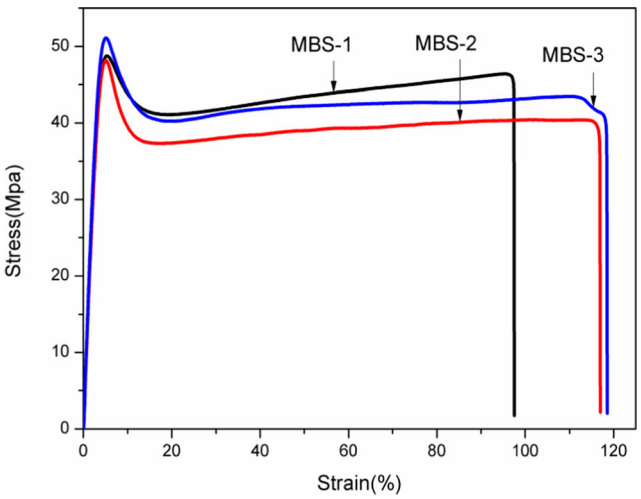

Fig. 6 Stress–strain curves of three different PVC/MBS blends

particles, G is the surface energy of the rubber phase, and the function F (λ_f) is dependent on the failure strain of the rubber under biaxial stretching conditions. The total energy U_r (r) of the cavitated particle is related the shear modulus and bulk modulus of the rubber. The model predicts that as stress is applied to a toughened polymer, the larger particles will cavitate easier.

In our experiments, the TEM samples were microtomed in the stress-whitening zone of the impact specimens to examine the deformation behavior immediately beneath the fracture surface. The ultrathin sections were cut parallel to the deformation direction. This allowed the observation of elongated particles and rubber cavitation, whenever they were present. Figure 7 shows the internal morphology of a stress-whitening zone in the Izod impact specimen. In the "salami" structure of MBS-1, the rubbery core was a PB homopolymer. Voiding was observed inside or around the rubber particles in the blend. Both internal cavitation and debonding coexisted in the sample. Dompas et al. [40] pointed that both the internal cavitation of the MBS particles and the debonding at the interface relieve the triaxial tension and therefore promote the shear yielding of the PVC matrix. For the "core-shell" two-layer MBS-2, the entire St was copolymerized with Bd in the core of MBS and led to a higher cavitation resistance. However, voids were detected inside the particles in the blend. In the MBS-3 particle, a glassy PS phase in the inner core provided the multi-interface of MBS and had a role in inducing the cavitation of the particles during the impact deformation of the PVC blend. When a multi-layer particle responded to an external applied strain, the soft rubber layer was easily elongated, whereas the PS core remained essentially underformed because of the higher Young's modulus. Furthermore, the adhesion between the sub-inclusions and PB was to a certain degree weak; as a result, voids appeared inside the particles. Thus, the multi-layer interface led the rubber to cavitate easily. In our study, the existence of hard PS glassy domains in the core acted as stiffening agents and led to a significant increase in tensile stress.

Table 3 The transmittance of the PVC/MBS blends

Sample	Transmittance (%)	Haze (%)
PVC/MBS-1	68.2	9.2
PVC/MBS-2	77.5	5.1
PVC/MBS-3	56.0	9.1

Transparency of the PVC/MBS blends

Therefore, the matching of the refractive index of MBS with that of PVC is a very important parameter for transparency. As Table 3 shows, the MBS with the same chemical composition but different internal structure leads to the difference in transparency. When the core of MBS was PB homopolymer, part of the St monomer swells into the PB rubbery phase and forms sub-inclusions. This leads to a serious local optical inhomogeneity in the core. For the MBS-3, the three-layer structure can be diminished to a minimum. Thus, MBS-2 has a higher transmittance than the others.

Conclusion

The variation of the core-shell particles and the properties of PVC/MBS blends were investigated in this work. Microscopic studies by TEM showed that the three MBS samples have different internal structures and that cavitation and debonding from the matrix easily take place in the blend. The results of the DMA illustrated that the variation in the core affects the glass transition temperature of the rubbery phase and the storage modulus of the core-shell particles. The results of the Izod impact tests showed that PVC/MBS-3 has the lowest BDT

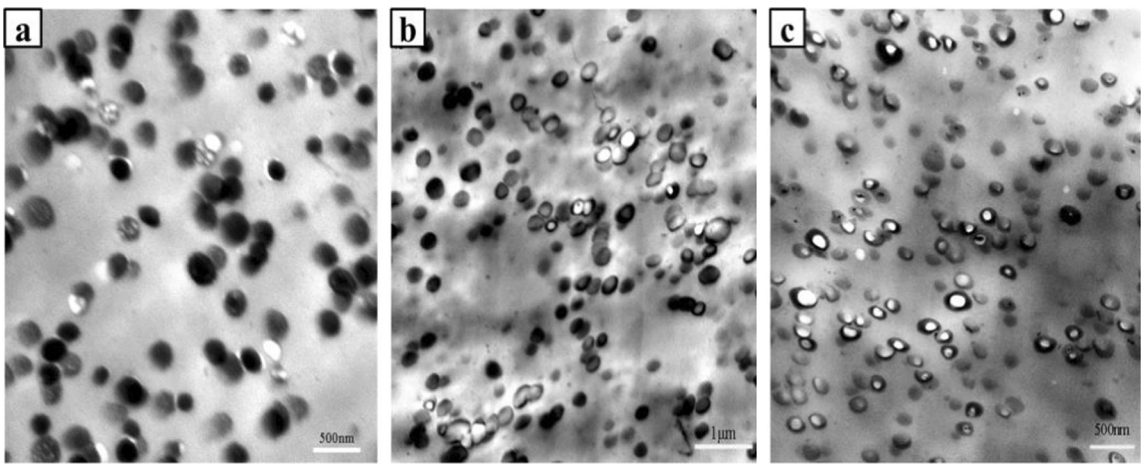

Fig. 7 TEM micrographs of stress-whitening zone in PVC/MBS blends under impact test: **a** PVC/MBS-1; **b** PVC/MBS-2; **c** PVC/MBS-3

temperature and that the PVC can maintain a higher tensile strength and stress with an increase in the rubbery volume fraction. The transparency test revealed that the presence of sub-inclusions in the rubbery phase can reduce the transparency of the blend.

Acknowledgments This project was financially supported by the Natural Science Foundation of China (51003007 and 50803007)

Contract grant sponsor Natural Science Foundation of China; contract Grant numbers: 51173020 and 51003007

References

1. Bucknall CB (1997) In: Haward RN, Young RJ (eds) The physics of glassy polymers, 2nd edn. Chapman & Hall, London
2. Michler GH (1992) Carl Hanser-Verlag, München
3. Bucknall CB (1977) Toughened plastics. Applied Science, London
4. Michler GH (1994) Acta Polym 44:113–124
5. Connor BO, Bucknall CB, Hahnfeld JL (1997) Plast Rubber Compos Process Appl 26:360–367
6. Michler GH, Starke JU (1996) In: Riew CK, Kinloch AJ (eds) Toughened plastics II, vol 17. American Chemical Society, Washington DC, pp 251–277
7. Bucknall CB (2000) In: Paul DR, Bucknall CB (eds) Ploymer blends, vol 2. Wiley, New York, pp 83–117, Ch. 22
8. Archer AC, Lovell PA, McDonald J, Sherratt MN, Young (1992) MRS Proc 274:17
9. Ayre DS, Bucknall CB (1998) Polymer 39:4785–4791
10. Abu-Isa IA, Jaynes CB, O'Gara JF (1996) J Appl Polym Sci 59: 1957–1971
11. Memon NA (1998) J Polym Sci B Polym Phys 36:1095–1105
12. Yu ZZ, Ou YC, Qi ZN, Hu GH (1998) J Polym Sci B Polym Phys 36:1987–1994
13. Lin KF, Shieh YD (1998) J Appl Polym Sci 70:2313–2322
14. Bucknall CB, Cote FFP, Partridge IK (1986) J Mater Sci 21: 301–306
15. Williams JG, Ford H (1964) J Mech Eng Sci 6:405–417
16. Herrera V, Palmillas Z, Pirri R, Reyes Y, Jose RL, Jose MA (2010) Macromolecules 43:1356–1363
17. The B.F. Goodrich Co., WO 93/21274(Oct. 28, 1993)
18. Gao G, Zhou C, Yang H, Zhang H (2007) J Appl Polym Sci 103: 738–744
19. Dong W, Cao X, Li Y (2014) Polym Int 63:1094–1100
20. Daniel JC (1985) Die Makromol Chem 10:359–390
21. Okubo M (1990) Makronmol Chem Macromol Symp 35–36: 307–325
22. Lovell PA, McDonald J, Saunders DEJ, Young RJ (1993) Polymer 34:61–69
23. Nelliappan V, EL-Aasser MS, Klein A, Daniels ES, Roberts JE, Pearson RA (1997) J Appl Polym Sci 65:581–593
24. Schneider M, Pith T, Lambla M (1997) J Mater Sci 32:6331–6342
25. Schneider M, Pith T, Lambla M (1997) J Mater Sci 32:6343–6356
26. Zhou C, Chen M, Tan Z, Sun S, Ao Y, Zhang M, Yang H, Zhang H (2006) Eur Polym J 42:1181–1818
27. Si QB, Zhou C, Yang HD, Zhang HX (2007) Eur Polym J 43: 3060–3067
28. Yang B, Chen M, Wang C, Wu GF, Zhang H, Zhou C (2014) J Polym Res 21:1–7
29. Pusch J, van Herk AM (2005) Macromolecules 38:6909–6914
30. Guo TY, Yang GL, Hao GJ, Song MD, Zhang BH (2003) J Appl Polym Sci 90:1290–1297
31. Tolue S, Reza MM, Mehdi GS (2009) Eur Polym J 45:714–720
32. Morbitzer L, Kranz D, Humme G, Ott KH (1976) J Appl Polym Sci 20:2691–2704
33. Wagner ER, Robeson LM (1970) Rubber Chem Technol 43: 1129–1137
34. Bucknall CB, Davies P, Partridge IK (1986) J Mater Sci 21: 307–313
35. Zuiderduin WCJ, Vlasveld DPN, Huetink J, Gaymans RJ (2004) Polymer 45:3765–3776
36. Pearson RA, Yee AF (1986) J Mater Sci 21:2475–2488
37. Pearson RA, Yee AF (1989) J Mater Sci 24:2571–2580
38. Pearson RA, Yee AF (1991) J Mater Sci 26:3828–3844
39. Lazzeri A, Bucknall CB (1995) Polymer 36:2895–2904
40. Dompas D, Groeninckx G, Isogawa M, Hasegawa T, Kadokura M (1995) Polymer 36:437–441